Seeing Beyond Lambert's Law

Michael Oren and Shree K. Nayar

Department of Computer Science, Columbia University, New York, N.Y. 10027, U.S.A

Abstract: Lambert's model for diffuse reflection is extensively used in computational vision. For several real-world objects, the Lambertian model can prove to be a very inaccurate approximation to the diffuse component. While the brightness of a Lambertian surface is independent of viewing direction, the brightness of a rough diffuse surface increases as the viewer approaches the source direction. A comprehensive model is developed that predicts reflectance from rough diffuse surfaces. Experiments have been conducted on real samples, such as, plaster, clay, and sand. The reflectance measurements obtained are in strong agreement with the reflectance predicted by the proposed model.

1 Introduction

A surface that obeys Lambert's Law appears equally bright from all viewing directions [Lambert-1760]. This model for diffuse reflection was advanced by Lambert over 200 years ago and remains one of the most widely used models in machine vision. It is used explicitly by shape recovery techniques such as shape from shading and photometric stereo. It is also invoked by vision techniques such as binocular stereo and motion detection to solve the correspondence problem. For several real-world objects, however, the Lambertian model can prove to be a poor and inadequate approximation to the diffuse component. It is shown in this paper, that surface roughness plays a critical role in the deviation from Lambertian behavior. This deviation is significant for very rough surfaces, and increases with the angle of incidence.

The topic of rough diffuse surfaces has been extensively studied in the areas of applied physics and geophysics. The following is a very brief summary of previous results on the subject. In 1924, Opik [Öpik-1924] designed an empirical model to describe the non-Lambertian behavior of the moon. In 1941, Minnaert [Minnaert-1941] modified Opik's model to obtain the following reflectance function:

$$f_r = \frac{k+1}{2\pi}(\cos\theta_i \cos\theta_r)^{(k-1)} \qquad (0 \leq k \leq 1)$$

where, θ_i and θ_r are the polar angles of incidence and reflection, and k is a measure of surface roughness. This function was designed to obey Helmholtz's reciprocity principle but is not based on any theoretical foundation. It assumes that the radiance of non-Lambertian diffuse surfaces is symmetrical with respect to the surface normal, an assumption that proves to be incorrect.

The above studies were attempts to design reflectance models based on measured reflectance data. In contrast, several investigators developed theoretical models for diffuse reflection from rough surfaces (see [Oren and Nayar-1992] for a more detailed survey). These efforts were motivated primarily by the reflectance characteristics of the moon. Infrared emission and visible light reflection from

the moon indicate that the moon's surface radiates more energy back in the direction of the source (the sun) than in the normal direction (like Lambertian surfaces) or in the forward direction (like specular surfaces). This phenomenon is referred to as *backscattering*[1]. Though several models were developed to describe this phenomenon [Smith-1967] [Buhl *et al.*-1968] [Hering and Smith-1970], these models are limited either because they assume restrictive surface geometries, or because they are confined to reflections in the plane of incidence.

In contrast, the model presented here can be applied to isotropic as well as anisotropic rough surfaces, and can handle arbitrary source and viewer directions. Further, it takes into account complex geometrical effects such as *masking*, *shadowing*, and *interreflections* between points on the surface. We begin by modeling the surface as a collection of long symmetric V-cavities with Lambertian facets. First, a reflectance model is developed for anisotropic surfaces with one type (facet-slope) of V-cavities, and with all cavities aligned in the same direction on the surface plane. This result is then used to derive a model for the more general case of isotropic surfaces that have normal facet distributions with zero mean and arbitrary standard deviation (σ). The standard deviation parametrizes the macroscopic roughness of the surface. The Lambertian model is a special case, or instance, of the derived model.

Figure 1 shows three images of spheres rendered using the proposed reflectance model. In all three cases, the sphere is illuminated from the viewer direction. In the first case, $\sigma = 0$, and hence the sphere is Lambertian in reflectance. As the roughness increases, the sphere begins to appear flatter. In the extreme roughness case shown in Figure 1(c), the sphere appears like a flat disc with nearly constant brightness. This phenomenon has been widely observed and reported in the case of the full moon.

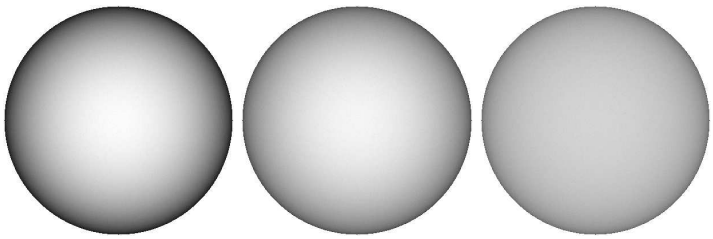

(a)Lambertian (b)$\sigma = 20°$ (c)$\sigma = 40°$

Fig. 1. Images of spheres rendered using the proposed reflectance model.

[1] A different backscattering mechanism produces a sharp peak close to the source direction (see [Hapke and van Horn-1963, Oetking-1966, Tagare and deFigueiredo-1991]). This is not the mechanism discussed in this paper. Hapke *et al.* [Hapke *et al.*-1993] attribute this backscatter peak to a physical-optics phenomenon called the "opposition effect." This phenomenon is seldom encountered in machine vision since it is observed only when the sensor and source are within a few degrees from each other; a situation difficult to emulate in practice without the source or the sensor occluding the other.

Several experimental results are presented to demonstrate the accuracy of the diffuse reflectance model. These experiments were conducted on commonplace samples such as sand and plaster. In all cases, reflectance predicted by the model was found to be in strong agreement with measurements. These results illustrate that the deviation from Lambertian behavior can be substantial. We conclude with a discussion on the implications of the proposed model for machine vision. Specifically, the effect of the described reflectance characteristics on image brightness, reflectance maps, and shape recovery algorithms is examined. These results demonstrate that the findings reported here are fundamental to the problem of visual perception.

2 Surface Roughness Model

The effects of shadowing, masking, and interreflection need to be analyzed in order to obtain an accurate reflectance model. To accomplish this, we use the roughness model proposed by Torrance and Sparrow [Torrance and Sparrow-1967] that assumes the surface to be composed of long symmetric V-cavities (see Figure 2). Each cavity consists of two planar facets. The width of each facet is assumed to be small compared to its length. We assume each facet area da is small compared to the area dA of the surface patch that is imaged by a single sensor pixel. Hence, each pixel includes a very large number of facets. Further, the facet area is large compared to the wavelength λ of incident light and therefore geometrical optics can be used to derive the reflectance model. The above assumptions can be summarized as: $\lambda^2 \ll da \ll dA$

We denote the slope and orientation of each facet in the V-cavity model as (θ_a, ϕ_a), where θ_a is the polar angle and ϕ_a is the azimuth angle. Torrance and Sparrow have assumed all facets to have equal area da. They use the distribution $N(\theta_a, \phi_a)$ to represent the number of facets per unit surface area that have the normal $\hat{a} = (\theta_a, \phi_a)$. Here, we use a probability distribution to represent the fraction of the surface area that is occupied by facets with a given normal. This is referred to as the *slope-area distribution* $P(\theta_a, \phi_a)$. The facet-number distribution and the slope-area distribution are related as follows:

$$P(\theta_a, \phi_a) = \frac{dA\ N(\theta_a, \phi_a)\ da\ \cos\theta_a}{dA} = N(\theta_a, \phi_a)\, da\ \cos\theta_a \tag{1}$$

The slope-area distribution is easier to use than the facet-number distribution in the following model derivation. For isotropic surfaces, $N(\theta_a, \phi_a) = N(\theta_a)$ and $P(\theta_a, \phi_a) = P(\theta_a)$, since the distributions are rotationally symmetric with respect to the global surface normal $\hat{n}$ (Figure 2).

3 Reflectance Model

In this section, we derive a reflectance model for rough diffuse surfaces. For lack of space, only important results are discussed. For details we refer the reader to [Oren and Nayar-1992]. During the derivation, we will draw on several well-known radiometric definitions that are given in [Nicodemus *et al.*-1977].

Consider a surface area dA that is imaged by a single sensor element in the direction $\hat{v} = (\theta_r, \phi_r)$ and illuminated by a distant point light source in the direction $\hat{s} = (\theta_i, \phi_i)$. The area dA is composed of a very large number of

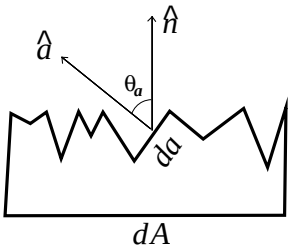

Fig. 2. Surface modeled as a collection of V-cavities.

symmetric V-cavities. Each V-cavity is composed of two facets with the same slope but facing in opposite directions. Consider the flux reflected by a facet with area da and normal $\hat{a} = (\theta_a, \phi_a)$. The projected area on the surface occupied by the facet is $da\,\cos\theta_a$ (see Figure 2). Thus, while computing the contribution of the facet to the radiance of the surface patch, we need to use the projected area $da\,\cos\theta_a$ and not the actual facet area da. This radiance contribution is what we call the *projected radiance* of the facet:

$$L_{rp}(\theta_a, \phi_a) = \frac{d\Phi_r(\theta_a, \phi_a)}{(da\cos\theta_a)\,\cos\theta_r\,d\omega_r} \tag{2}$$

where, $d\omega_r$ is the solid angle subtended by the sensor optics. For ease of description, we have dropped the source and viewing directions from the notations for projected radiance and flux. Now consider the slope-area distribution of facets given by $P(\theta_a, \phi_a)$. The total radiance of the surface can be obtained as the aggregate of $L_{rp}(\theta_a, \phi_a)$ over all facets on the surface:

$$L_r(\theta_r, \phi_r; \theta_i, \phi_i) = \int_{\theta_a=0}^{\frac{\pi}{2}} \int_{\phi_a=0}^{2\pi} P(\theta_a, \phi_a)\, L_{rp}(\theta_a, \phi_a)\, \sin\theta_a\, d\phi_a\, d\theta_a \tag{3}$$

3.1 Model for Uni-directional Single-Slope Distribution

The first surface type we consider has all facets with the same slope θ_a. Further, all V-cavities are aligned in the same direction; azimuth angles of all facets are either ϕ_a or $\phi_a + \pi$. Consider a Lambertian facet with albedo ρ, that is fully illuminated (no shadowing) and is completely visible (no masking) from the sensor direction. The radiance of the facet is proportional to its irradiance and is equal to $\frac{\rho}{\pi}E(\theta_a, \phi_a)$. The irradiance of the facet is $E(\theta_a, \phi_a) = E_0 < \hat{s}, \hat{a} >$, where, E_0 is the irradiance when the facet is illuminated head-on (i.e. $\hat{s} = \hat{n}$), and $<,>$ denotes the dot product between two vectors. Using the definition of radiance [Nicodemus *et al.*-1977], the flux reflected by the facet in the sensor direction is: $d\Phi_r = \frac{\rho}{\pi}E_0 < \hat{s}, \hat{a} >< \hat{v}, \hat{a} >$. Substituting this expression in (2), we get:

$$L_{rp}(\theta_a, \phi_a) = \frac{\rho}{\pi}E_0 \frac{< \hat{s}, \hat{a} >< \hat{v}, \hat{a} >}{< \hat{a}, \hat{n} >< \hat{v}, \hat{n} >} \tag{4}$$

The above expression clearly illustrates that the projected radiance of a tilted Lambertian facet is not equal in all viewing directions.

Geometric Attenuation Factor: If the surface is illuminated and viewed from the normal direction ($\hat{s} = \hat{v} = \hat{n}$), all facets are fully illuminated and visible. For larger angles of incidence and reflection, however, facets are shadowed and masked by adjacent facets (see Figure 3). Both these geometrical phenomena reduce the projected radiance of the facet. This reduction in brightness can be derived using geometry and incorporated into a single term, called the *geometrical attenuation factor* ($\mathcal{GAF}$), that lies between zero and unity. Several derivations of the $\mathcal{GAF}$ have been presented [Torrance and Sparrow-1967] [Blinn-1977] [Oren and Nayar-1992]. The final result can be compactly represented as:

$$\mathcal{GAF} \;=\; Min\left[1,\, Max\left[0,\, \frac{2<\hat{s},\hat{n}><\hat{a},\hat{n}>}{<\hat{s},\hat{a}>},\, \frac{2<\hat{v},\hat{n}><\hat{a},\hat{n}>}{<\hat{v},\hat{a}>}\right]\right] \qquad (5)$$

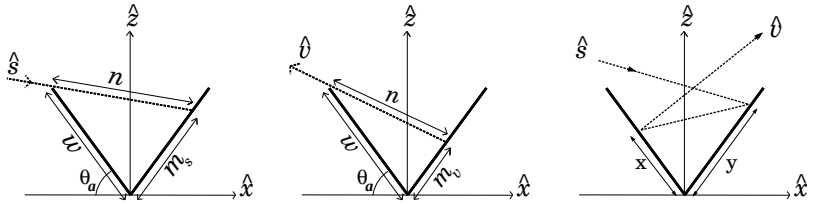

(a) Shadowing (b) Masking (c) Interreflection

Fig. 3. Shadowing, masking, and interreflection in a V-cavity

Projected Radiance and $\mathcal{GAF}$: The projected radiance of a Lambertian facet is obtained by multiplying the $\mathcal{GAF}$ with the projected radiance given by (4). Table 1 details the $\mathcal{GAF}$ and the corresponding projected radiance for all cases of shadowing and masking. Note that the projected radiance is denoted as L^1_{rp}; the superscript is used to indicate that the radiance is due to direct illumination by the source. In the following discussion, we will use L^2_{rp} to denote radiance due to interreflections.

Table 1. Projected radiance of a facet for different masking/shadowing conditions.

	$\mathcal{GAF}$	$L^1_{rp}(\theta_a, \phi_a)$
No Masking or Shadowing	1	$\frac{\rho}{\pi} E_0 \frac{<\hat{s},\hat{a}><\hat{v},\hat{a}>}{<\hat{a},\hat{n}><\hat{v},\hat{n}>} =$ $\frac{\rho}{\pi} E_0 \cos\theta_i \cos\theta_a \Big(1 + \tan\theta_i \tan\theta_a \cos(\phi_i - \phi_a)\Big)$ $\Big(1 + \tan\theta_r \tan\theta_a \cos(\phi_r - \phi_a)\Big)$
Masking	$\frac{2<\hat{v},\hat{n}><\hat{a},\hat{n}>}{<\hat{v},\hat{a}>}$	$\frac{\rho}{\pi} E_0 \, 2<\hat{s},\hat{a}> =$ $\frac{\rho}{\pi} E_0 \cos\theta_i \cos\theta_a \; 2\Big(1 + \tan\theta_i \tan\theta_a \cos(\phi_i - \phi_a)\Big)$
Shadowing	$\frac{2<\hat{s},\hat{n}><\hat{a},\hat{n}>}{<\hat{s},\hat{a}>}$	$\frac{\rho}{\pi} E_0 \frac{2<\hat{s},\hat{n}><\hat{v},\hat{a}>}{<\hat{v},\hat{n}>} =$ $\frac{\rho}{\pi} E_0 \cos\theta_i \cos\theta_a \; 2\Big(1 + \tan\theta_r \tan\theta_a \cos(\phi_r - \phi_a)\Big)$

Interreflection Factor: We have the task of modeling interreflections in the presence of masking and shadowing effects. In the case of Lambertian surfaces, the energy in an incident light ray diminishes rapidly with each interreflection bounce. Therefore, we model only two-bounce interreflections and ignore subsequent bounces. Since the length l of the V-cavity is much larger than its width w, i.e. $l \gg w$, it can be viewed as a one-dimensional shape with translational symmetry. For such shapes, the two-bounce interreflection component can be determined as an integral over the one-dimensional cross-section of the shape [Siegel and Howell-1972]:

$$L_r^2(x) = \frac{\rho}{\pi} \int K'(x,y) L_r^1(y) dy \tag{6}$$

where x and y are the shortest distances of facet points from the intersection of the two facets (see Figure 3(c)). K' is the kernel for the translational symmetry case and is derived in [Jakob-1957] and [Forsyth and Zisserman-1989] to be:

$$K'(x,y) = \frac{\pi \sin^2(2\theta_a)}{2} \frac{xy}{(x^2 + 2xy\cos(2\theta_a) + y^2)^{3/2}} \tag{7}$$

We know that the orientation of the considered facet is $\hat{a} = (\theta_a, \phi_a)$ and the orientation of the adjacent facet is $\hat{a}' = (\theta_a, \phi_a + \pi)$. The limits of the integral in the interreflection equation are determined by the masking and shadowing of these two facets. Let m_v be the width of the facet which is visible to the viewer, and m^s be the width of the *adjacent* facet that is illuminated. From the definitions of radiance and projected radiance we get:

$$L_{rp}^2 = \frac{l < \hat{a}, \hat{v} >}{da < \hat{a}, \hat{n} > < \hat{v}, \hat{n} >} \int_{x=m_v}^{w} L_r^2(x)\, dx \tag{8}$$

Using the following change of variables: $r = \frac{y}{w}$; $t = \frac{x}{w}$, the radiance due to two-bounce interreflections given by (6) and (8) can be written as:

$$L_{rp}^2 = (\frac{\rho}{\pi})^2 E_0 \frac{< \hat{a}', \hat{s} >< \hat{a}, \hat{v} >}{< \hat{a}, \hat{n} >< \hat{v}, \hat{n} >} \int_{t=\frac{m_v}{w}}^{1} \int_{r=\frac{m^s}{w}}^{1} K'(t,r) dr\, dt \tag{9}$$

Using (7), the above integral is evaluated as:

$$\int_{t=\frac{m_v}{w}}^{1} \int_{r=\frac{m^s}{w}}^{1} K'(r,t) dr\, dt = \frac{\pi}{2} \left[d(1, \frac{m_v}{w}) + d(1, \frac{m^s}{w}) - d(\frac{m^s}{w}, \frac{m_v}{w}) - d(1,1) \right] \tag{10}$$

where: $d(x,y) = \sqrt{x^2 + 2xy\cos(2\theta_a) + y^2}$. We refer to (10) as the *interreflection factor* ($\mathcal{IF}$). From (9), the interreflection component of the projected radiance of a facet with orientation (θ_a, ϕ_a) is:

$$L_{rp}^2(\theta_a, \phi_a) = (\frac{\rho}{\pi})^2 E_0 \cos\theta_i \cos\theta_a \tag{11}$$
$$\Big(1 - \tan\theta_i \tan\theta_a \cos(\phi_i - \phi_a)\Big) \Big(1 + \tan\theta_r \tan\theta_a \cos(\phi_r - \phi_a)\Big) \mathcal{IF}(\hat{v}, \hat{s}, \hat{a})$$

The total projected radiance of the facet is the sum of the projected radiance due to source illumination (given in Table 1) and the above interreflection component: $L_{rp}(\theta_a, \phi_a) = L_{rp}^1(\theta_a, \phi_a) + L_{rp}^2(\theta_a, \phi_a)$ The uni-directional single-slope surface considered here has only two types of facets with normals (θ_a, ϕ_a) and $(\theta_a, \phi_a + \pi)$. Hence, the radiance of the surface for any given source and sensor directions is simply the average of the projected radiances of the two facet types.

3.2 Model for Isotropic Single-Slope Distribution

All facets on this isotropic surface have the same slope θ_a but are uniformly distributed in ϕ_a. From the previous section, we know the radiance $L_{rp}(\theta_a, \phi_a)$ of a facet with normal $\hat{a} = (\theta_a, \phi_a)$. Therefore, the radiance of the isotropic surface is determined as an integral of the projected radiance over ϕ_a:

$$L_{rp}(\theta_a) = \frac{1}{2\pi} \int_{\phi_a=0}^{2\pi} L_{rp}(\theta_a, \phi_a) d\phi_a \tag{12}$$

Given a source direction (θ_i, ϕ_i) and a sensor direction (θ_r, ϕ_r), we first need to find the ranges of facet orientation ϕ_a for which the facets are masked, shadowed, masked and shadowed, and neither masked nor shadowed[2]. This requires a careful geometrical analysis. Once this is done the above integral can be decomposed into parts corresponding to masking/shadowing ranges. Each range is evaluated using the corresponding radiance expression in Table 1. We refer the interested reader to [Oren and Nayar-1992] for details on the evaluation of direct illumination and interreflection components of (12).

3.3 Model for Gaussian Slope-Area Distribution

In the case of isotropic surfaces, the slope-area distribution can be described using a single parameter, namely, θ_a, since the facets are uniformly distributed in ϕ_a. The radiance of any isotropic surface can therefore be determined as:

$$L_r(\theta_r, \theta_i, \phi_r - \phi_i) = \int_0^{\frac{\pi}{2}} P(\theta_a) L_{rp}(\theta_a) \sin\theta_a d\theta_a \tag{13}$$

where $L_{rp}(\theta_a)$ is the projected radiance obtained in the previous section. Here, we assume the isotropic distribution to be Gaussian with mean μ and standard deviation σ, i.e. $P(\theta_a; \sigma, \mu)$. Reasonably rough surfaces can be described using a zero mean ($\mu = 0$) Gaussian distribution: $P(\theta_a) = c\ exp\left(-\theta_a^2/2\sigma^2\right)$ where, the c is the normalization constant.

The above integral cannot be easily evaluated. Therefore, we pursued a functional approximation [Oren and Nayar-1992] to the integral that is accurate for arbitrary surface roughness and angles of incidence and reflection. The final approximation results are given below. Let $\alpha = Max[\theta_r, \theta_i]$ and $\beta = Min[\theta_r, \theta_i]$. The source illumination component of radiance of a surface with roughness σ is:

$$L_r^1(\theta_r, \theta_i, \phi_r - \phi_i; \sigma) = \frac{\rho}{\pi} E_0 \cos\theta_i \left[C_1(\sigma) + \right. \tag{14}$$
$$\left. \cos(\phi_r - \phi_i) C_2(\alpha; \beta; \phi_r - \phi_i; \sigma) \tan\beta + \left(1 - |\cos(\phi_r - \phi_i)|\right) C_3(\alpha; \beta; \sigma) \tan\left(\frac{\alpha+\beta}{2}\right) \right]$$

where the coefficients are:

$$C_1 = 1 - 0.5 \frac{\sigma^2}{\sigma^2 + 0.33}$$

$$C_2 = \begin{cases} 0.45 \frac{\sigma^2}{\sigma^2+0.09} \sin\alpha & \text{if } \cos(\phi_r - \phi_i) \geq 0 \\ 0.45 \frac{\sigma^2}{\sigma^2+0.09} \left(\sin\alpha - (\frac{2\beta}{\pi})^3\right) & \text{otherwise} \end{cases}$$

$$C_3 = 0.125 \left(\frac{\sigma^2}{\sigma^2 + 0.09}\right) \left(\frac{4\alpha\beta}{\pi^2}\right)^2$$

[2] Imagine a V-cavity rotated about the global surface normal for any given source and sensor direction. Various masking/shadowing scenarios can be visualized.

Using a similar approach, an approximation to the interreflection component was also derived:

$$L_r^2(\theta_r, \theta_i, \phi_r - \phi_i; \sigma) = 0.17 \frac{\rho^2}{\pi} E_0 \cos\theta_i \frac{\sigma^2}{\sigma^2 + 0.13} \left[1 - \cos(\phi_r - \phi_i) \left(\frac{2\beta}{\pi} \right)^2 \right] \quad (15)$$

The two components are combined to obtain the total surface radiance: $L_r(\theta_r, \theta_i, \phi_r - \phi_i; \sigma) = L_r^1(\theta_r, \theta_i, \phi_r - \phi_i; \sigma) + L_r^2(\theta_r, \theta_i, \phi_r - \phi_i; \sigma)$. Finally, the *BRDF* of the surface is obtained from its radiance and irradiance as $f_r(\theta_r, \theta_i, \phi_r - \phi_i; \sigma) = L_r(\theta_r, \theta_i, \phi_r - \phi_i; \sigma) \,/\, E_0 \cos\theta_i$. It is important to note that the above model obeys Helmholtz's reciprocity principle. *Also note that the model reduces to the Lambertian model when* $\sigma = 0$.

Qualitative Model: A further simplification to the above model can be achieved with a slight sacrifice in accuracy. The following model was arrived at by studying, through numerous simulations, the relative contributions of various terms in the functional approximation given by (14). The simulations showed that coefficient C_3 makes a relatively small contribution to the total radiance. A simpler model is thus obtained by discarding C_3 and ignoring interreflections:

$$L_r(\theta_r, \theta_i, \phi_r - \phi_i; \sigma) = \frac{\rho}{\pi} E_0 \cos\theta_i (C_1 + C_2 Max\left[0, \cos(\phi_r - \phi_i)\right] \tan\beta) \quad (16)$$

This model can be of significant practical value in applications where very high accuracy is not critical.

4 Experiments

We have conducted several experiments to verify the accuracy of the diffuse reflectance model. The experimental set-up used to measure the radiance of samples is described in [Oren and Nayar-1992]. Figures 4 and 5 shows results obtained for samples of wall plaster (A) and sand (B). The radiance of each sample is plotted as a function of sensor direction θ_r for different angles of incidence θ_i. These measurements are made in the plane of incidence ($\phi_r = \phi_i = 0$). For these two samples (A and B), σ and ρ were selected empirically to obtain the best match between measured and predicted reflectance. Here, we have used the numerical evaluation of the model (equation 13). For both samples, radiance increases as the viewing direction θ_r approaches the source direction θ_i (backward reflection). This is in contrast to the behavior of rough specular surfaces that reflect more in the forward direction, or Lambertian surfaces where radiance does not vary with viewing direction. For both samples, the model predictions and experimental measurements match remarkably well. In both cases, a small peak is noticed near the source direction. This phenomenon, known as the opposition effect [Hapke and van Horn-1963], was discussed earlier in the introduction and is different from the one described by our model.

Figure 6 shows results for a sample (foam) that has not only a diffuse component but also a significant specular component. In this case, the reflectance model used is a linear combination of new model and the Torrance-Sparrow model [Torrance and Sparrow-1967] that describes specular, or surface, reflection from rough surfaces: $L_r = k_d L_r^d + k_s L_r^s$ where L_r^d and L_r^s are the diffuse and specular components, respectively, and k_d and k_s are weighting coefficients

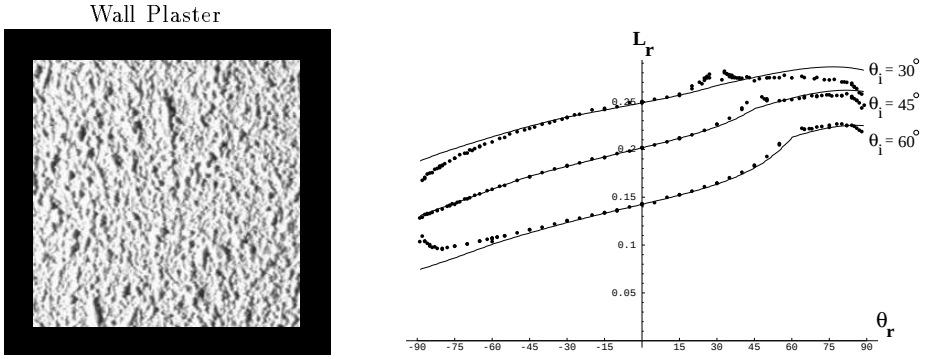

Fig. 4. Reflectance measurement (dots) and reflectance model (solid lines) ($\sigma = 30°$, $\rho = 0.90$) plots for wall plaster (sample A). Radiance is plotted as a function of sensor direction (θ_r) for different angles of incidence ($\theta_i = 30°, 45°, 60°$).

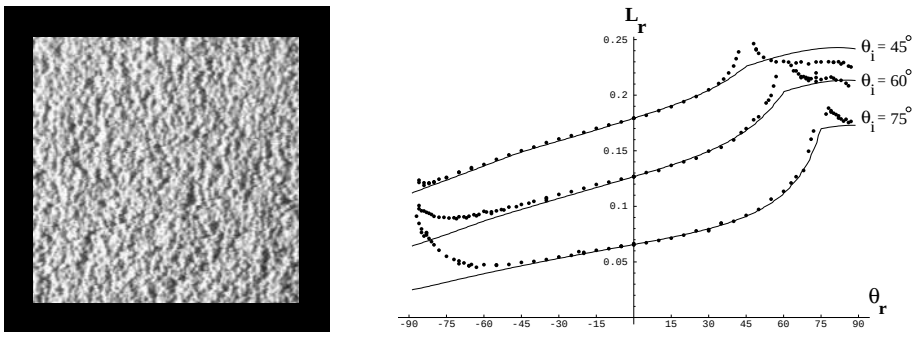

Fig. 5. Reflectance measurement and reflectance model ($\sigma = 35°$, $\rho = 0.80$) plots for sand (sample B).

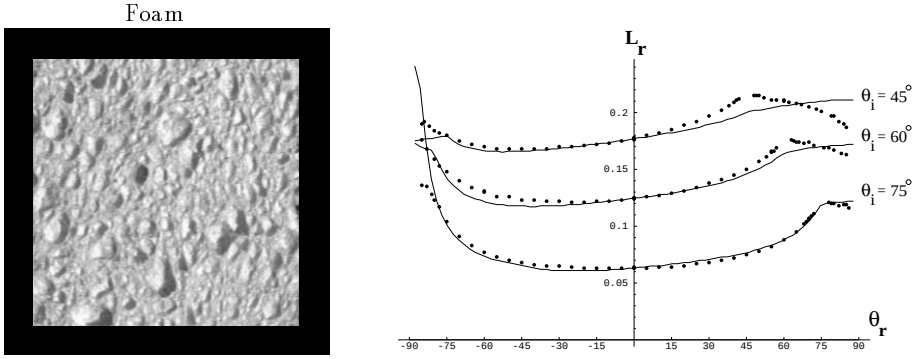

Fig. 6. Reflectance measurement and reflectance model ($\sigma = 20°$, $\rho = 0.8$, $k_s/k_d = 0.02$) plots for foam (sample C). The reflectance model used includes a specular component.

for the two components. For this experiment, we used the functional approximation (14) and the reflectance parameters σ, ρ, k_d, and k_s were estimated by fitting (using non-linear optimization) the model (14) to measured data. Other experiments based on the combined model are reported in [Oren and Nayar-1992].

5 Implications for Machine Vision

Numerous algorithms in computer vision use assumptions regarding reflectance properties of objects in the scene. Incorrect modeling of reflectance properties naturally leads to inaccurate results. We begin by examining images of rough diffuse surfaces. Figure 7(a) shows an image of the rough cylindrical clay vase taken using a CCD camera. The vase is illuminated by a single light source close to the sensor direction. Clearly, the real vase appears much flatter, with less brightness variation along its cross-section, than the Lambertian vase. Note that the proposed model does well in predicting the appearance of the vase. Here, roughness and albedo were selected empirically; $\sigma = 40°$ and $\rho = 0.70$. Figure 7(d) compares brightness values along the cross-section of the three different vase images. Note that the brightness of the real vase remains nearly constant over most of the cross-section and drops quickly to zero very close to the limbs. The proposed model does very well in predicting this behavior, while the Lambertian model produces large brightness errors.

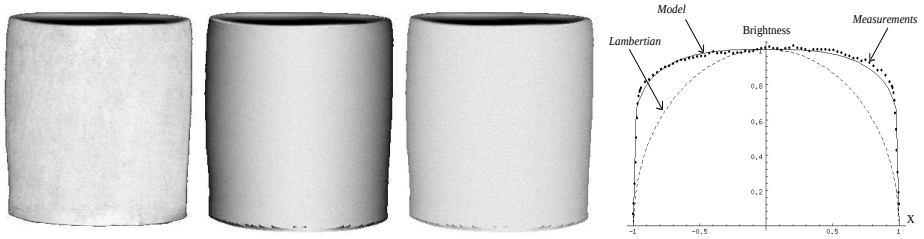

(a) Image (b) Lambertian (c) Model (d)

Fig. 7. (a-c) Real image of a cylindrical clay vase compared with images rendered using the Lambertian and proposed models. Illumination is from the direction $\theta_i = 0°$. (d) Comparison between image brightness along the cross-sections of the three vases.

Reflectance maps are widely used in vision for obtaining shape information from brightness images [Horn and Brooks-1989]. For a given reflectance model and source direction, the reflectance map establishes the relationship between surface orientation, given by the gradient space parameters (p, q), and image brightness. Figure 8(a) shows the reflectance map of a Lambertian surface for illumination from the direction $(\theta_i = 10°, \phi_i = 45°)$. The same reflectance map is obtained using the proposed model with roughness $\sigma = 0$. Figure 8(b) shows the reflectance map of a rough Lambertian surface with $\sigma = 60°$. Note that the rough Lambertian surface produces a map that appears very similar to the linear reflectance map [Horn and Brooks-1989] hypothesized for the lunar surface.

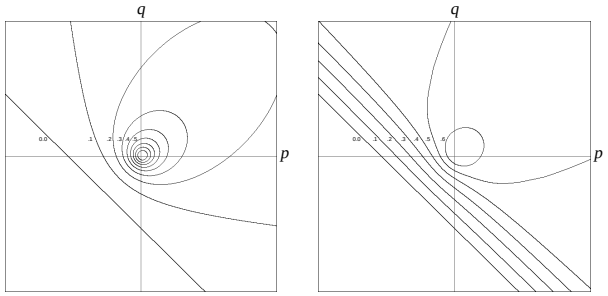

(a) Lambertian (b) Rough Lambertian

Fig. 8. Reflectance maps for (a) Lambertian surface ($\rho = 0.9$), and (b) rough Lambertian surface ($\sigma = 60°$, $\rho = 0.9$). For both maps the angles of incidence are $\theta_i = 10°$ and $\phi_i = 45°$. Note the similarity between the second map and the well-known linear reflectance map previously suggested for lunar reflectance.

The proposed reflectance model therefore establishes a continuum from pure Lambertian to lunar-like reflectance.

The problem of recovering shape from brightness images has been intensely researched in the past two decades. Several algorithms have been proposed, the most noteworthy of these being shape from shading [Horn and Brooks-1989] and photometric stereo [Woodham-1980]. For these methods to produce meaningful shape estimates, it is imperative that accurate reflectance models be used. Here, we present results obtained by applying photometric stereo to the clay vase shown in Figure 7. Figure 9(a) shows the shape of the vase recovered using the Lambertian model, and Figure 9(b) shows the shape computed using the proposed model with the same roughness and albedo used to render the image in Figure 7(c). Figure 9(c) compares height values computed along the vase cross-section using the two models. It is evident from this plot that the Lambertian model results in large errors in computed orientation and hence also in computed height. Similar errors are expected in the case of shape from shading.

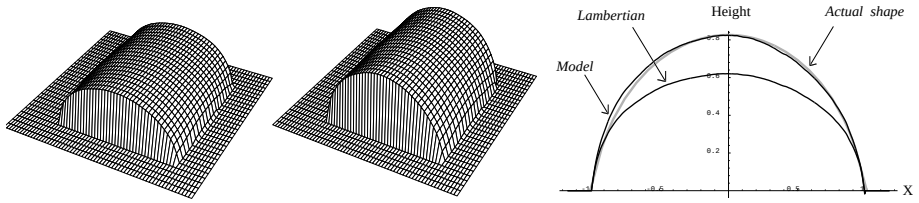

(a) Lambertian (b) Model (c) Cross section

Fig. 9. Shape of the vase in Figure 7(a) determined by photometric stereo using (a) the Lambertian model, and (b) the proposed model. In both cases, images were obtained using two light sources at angles $-10°$ and $10°$ with respect to the sensor direction. (c) Actual profile of the vase compared with profiles computed using the Lambertian model and the proposed model ($\sigma = 40°$, $\rho = 0.70$). The Lambertian model produces large errors in computed shape.

References

[Blinn, 1977] J. F. Blinn. Models of light reflection for computer synthesized pictures. *ACM Computer Graphics (SIGGRAPH 77)*, 19(10):542–547, 1977.

[Buhl *et al.*, 1968] D. Buhl, W. J. Welch and D. G. Rea. Reradiation and thermal emission from illuminated craters on the lunar surface. *Journal of Geophysical Research*, 73(16):5281–5295, August 1968.

[Forsyth and Zisserman, 1989] D. Forsyth and A. Zisserman. Mutual illumination. *Proc. Conf. Computer Vision and Pattern Recognition*, pages 466–473, 1989.

[Hapke and van Horn, 1963] B. W. Hapke and Huge van Horn. Photometric studies of complex surfaces, with applications to the moon. *Journal of Geophysical Research*, 68(15):4545–4570, August 1963.

[Hapke *et al.*, 1993] B. W. Hapke, R. M. Nelson and W. D. Smythe. The opposition effect of the moon: The contribution of coherent backscatter. *Science*, 260(23):509–511, April 1993.

[Hering and Smith, 1970] R. G. Hering and T. F. Smith. Apparent radiation properties of a rough surface. *AIAA Progress in Astronautics and Aeronautics*, 23:337–361, 1970.

[Horn and Brooks, 1989] B. K. P. Horn and M. J. Brooks, editors. *Shape from Shading*. The MIT Press, 1989.

[Jakob, 1957] M. Jakob. *Heat Transfer*. Wiley, 1957.

[Lambert, 1760] J. H. Lambert. Photometria sive de mensure de gratibus luminis, colorum umbrae. *Eberhard Klett*, 1760.

[Öpik, 1924] E. Öpik. Photometric measures of the moon and the moon the earthshine. *Publications de L'Observatorie Astronomical de L'Universite de Tartu*, 26(1):1–68, 1924.

[Minnaert, 1941] M. Minnaert. The reciprocity principle in lunar photometry. *Astrophysical Journal*, 93:403–410, 1941.

[Nicodemus *et al.*, 1977] F. E. Nicodemus, J. C. Richmond and J. J. Hsia. *Geometrical Considerations and Nomenclature for Reflectance*. National Bureau of Standards, October 1977. Monograph No. 160.

[Oetking, 1966] P. Oetking. Photometric studies of diffusely reflecting surfaces with application to the brightness of the moon. *Journal of Geophysical Research*, 71(10):2505–2513, May 1966.

[Oren and Nayar, 1992] M. Oren and S. K. Nayar. Generalization of the lambertian model and implications for machine vision. Technical Report CUCS-057-92, Department of Computer Science, Columbia University, New York, NY, USA, 1992.

[Siegel and Howell, 1972] R. Siegel and J. R. Howell. *Thermal Radiation Heat Transfer*. Hemisphere Publishing Corporation, third edition, 1972.

[Smith, 1967] B. G. Smith. Lunar surface roughness: Shadowing and thermal emission. *Journal of Geophysical Research*, 72(16):4059–4067, August 1967.

[Tagare and deFigueiredo, 1991] H. D. Tagare and R. J. P. deFigueiredo. A theory of photometric stereo for a class of diffuse non-Lambertian surfaces. *IEEE Transactions on Pattern Analysis and Machine Intelligence*, 13(2):133–152, February 1991.

[Torrance and Sparrow, 1967] K. Torrance and E. Sparrow. Theory for off-specular reflection from rough surfaces. *Journal of the Optical Society of America*, 57:1105–1114, September 1967.

[Woodham, 1980] R. J. Woodham. Photometric method for determining surface orientation from multiple images. *Optical Engineering*, 19(1):139–144, January-February 1980.

This article was processed using the LaTeX macro package with LLNCS style